IR Spectroscopy

While NMR gave information about connectivity of atoms based on the odd spins of certain atomic nuclei (e.g. ^{1}H, ^{13}C, ^{15}N), IR gives information about various functional groups present in the molecule.

The infrared (IR) frequency range of the spectrum leads to vibrational spectroscopy. It has been discussed earlier (c.f. Figure 6.11) that for an n-atomic molecule there are 3n-6 vibrational modes at motion. This is the result of the following consideration. Each atom needs 3 coordinates (x,y,z) to specify its whereabouts in a 3D-space. For an n-atomic molecule this amounts to 3n coordinates. Of these 3n coordinates, 3 are reserved for translation and 3 are reserved for rotation, which leaves 3n-6 coordinates for internal motions i.e. for vibrations. The three translational and three rotational modes of motion are illustrated for the H_2O molecule in Figure 13.23. Thus for the case of H_2O, there are 3n-6 = 3 x 3 - 6 = 9 - 6 = 3 vibrational modes. Intuitively, one may consider that each of the two O - H bonds may be stretched and there may be an H - O - H bond bend. Actually, the two bond stretches are combined to give symmetric (ν_1) and antisymmetric (ν_3) stretches, while the bend (ν_2) remains to be a symmetric mode of motion. These fundamental vibrations are illustrated in Figure 13.24.

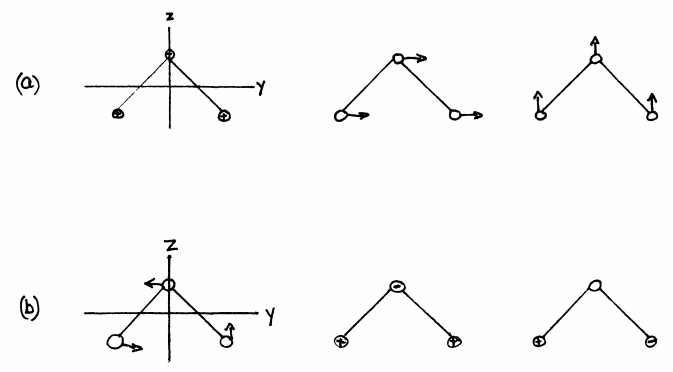

Figure 13.23 Translations (a) and rotations (b) of H_2O.

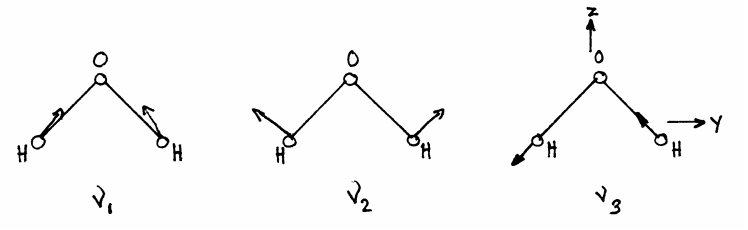

Figure 13.24 The normal vibrations of the H_2O molecule. The fundamental frequencies of the three modes of motions are denoted as ν_1, ν_2 (symmetric) and ν_3 (antisymmetric).

In general, the 3n-6 vibrational modes can be subdivided into three types of deformations: stretch, bend and torsion (see for example Figures 1.6 and 1.11). The approximate potential energy functions associated with these three types of modes of motion are shown, again schematically, in Figure 13.25.

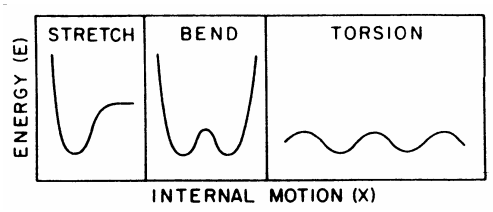

Figure 13.25 Three types of potentials associated with three types of internal modes of motion.

The energy requirement is the greatest for the stretch and the smallest for the torsion. Therefore, these three types fall into three different frequency ranges, even though there is some overlap (c.f. Figure 13.26).

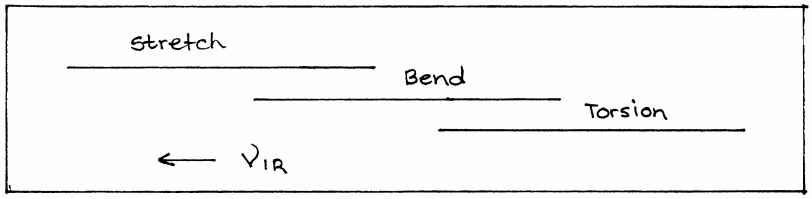

Figure 13.26 Overlapping frequency ranges for stretching, bending and torsional modes of vibration.

The formaldehyde molecule, which is also planar, has six normal vibrations (3n - 6 = 3 x 4 - 6 = 12 - 6 = 6) which can be represented approximately as follows:

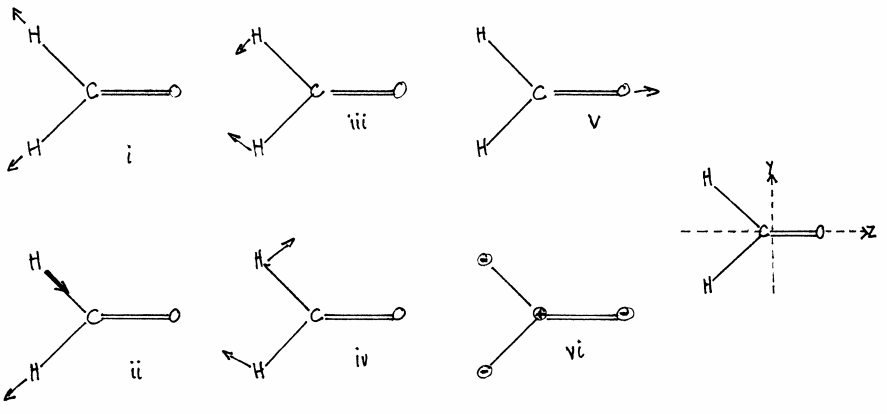

Figure 13.27 Six fundamental vibrations of formaldehyde.

Note that the first five of these modes (I - V) are in the plane of the molecule while the sixth (i.e. VI) is an out of plane vibration, deforming the molecule into a pyramidal geometry. The most typical fundamental frequency of vibration is associated with the fifth (i.e. V) mode which is the carbonyl stretching. For a carbonyl functional group the stretching mode usually falls in the range of 1600 - 1700cm^{-1}.

Characteristic stretching and bending frequencies of the most frequently occurring functional groups are shown in Table 13.3. The torsional frequencies (included in Table 13.3) are usually below $100 cm^{-1}$.

Table 13.3 Typical stretching and bending vibrational wave numbers.

Functional group	$\nu^*(cm^{-1})$	Functional group	$\nu^*(cm^{-1})$
Bond stretching		Bond stretching	
C≡C–H	3300	–C(–)–Br	560
C=C(H)–	3020	–C(–)–I	500
O=C(H)–	2800	–O–H	3600[a]
–C(–)–H	2960	–N(–)–H	3350
–C≡C–	2050	–P(–)=O	1295
–C(–)=C(–)–	1650	–S(–)=O	1310
–C(–)–C(–)–	900	Bond angle bending	
–Si(–)–Si(–)–	430	≡C–H	700
–C(–)=O	1700	=C(H)–H	1100
–C≡N	2100	–C(H)(H)–H	1000
–C(–)–F	1100	–C(H)(H)–	1450
–C(–)–Cl	650	C≡C–C	300

[a] In the absence of hydrogen bonding

To correspond to the minima of each of the three types vibrational potential energy curves (Figure 13.25), one can fit a parabola as illustrated schematically in Figure 13.28 for the stretching mode. The parabola represents a harmonic vibration, which is a fairly good approximation, close to the minimum, to the otherwise inharmonic vibration.

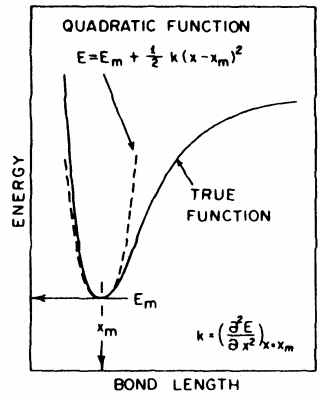

Figure 13.28 The approximation of the true stretching potential (solid curve) with the quadratic potential (broken curve) at the vicinity of the minimum energy point.

The quadratic equation (frequently referred to as Hooke's law) is a parabola:

[13.27]

where k is the force constant. The force constant determines the steepness of the potential function. If k is large, then the parabola is steep; if k is small, then the parabola is shallow.

The force constant also predetermines the IR frequency (ν)

[13.28]

where μ is the reduced mass. Thus, a large k means high frequency and a small k means low frequency.

The potential energy curve has vibrational levels. The lowest of these energy levels is the zero point vibrational level (E_{ZPV}) which is also related to the frequency. For a harmonic osscillator:

$$E_{ZPV} = \frac{1}{2}h\nu = \frac{1}{2}hc\nu^* \qquad [13.29]$$

$$\Delta E_{0\to1} = h\nu_{IR} = hc\nu^* \qquad [13.30a]$$

where [13.30] denotes the energy change associated with the IR transition from the zero point to the first vibrational levels (c.f. Figure 13.29).

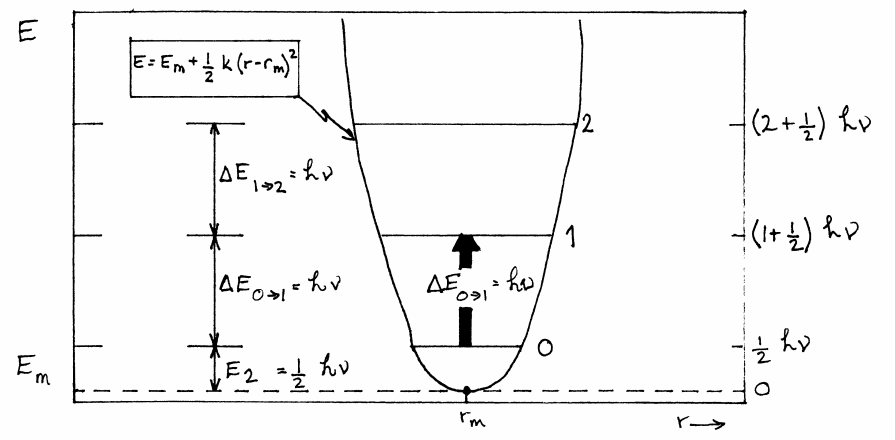

Figure 13.29 Vibrational energy levels of a harmonic potential.

Each of the vibrational modes may be characterized by a potential curve such as the one shown in Figure 13.29. Transitions along each of these modes contribute a peak to the IR spectrum.

If excitation occurs, simultaneously, along two vibrational modes, one with vibrational wave number ν_1^* and the other with ν_2^* then we obtain a *combination band* with a position corresponding to a value which is the sum of the two wave numbers: $(\nu_1^* + \nu_2^*)$. The excitation energy will therefore be

$$\Delta E_{combination} = hc\,(\nu_1^* + \nu_2^*) \qquad [13.30b]$$

In certain cases, these two frequencies may be associated with the same vibrational mode but the first one is corresponding to the $0 \rightarrow 1$ transition (i.e. $\nu_1^* = \nu^*_{0\rightarrow1}$) and the second one is corresponding to the $1\rightarrow2$ transition (i.e. $\nu_2^* = \nu^*_{1\rightarrow2}$). In such a case we have what is called an *overtone bond:* $(\nu^*_{0\rightarrow1} + \nu^*_{1\rightarrow2})$. If these two frequencies (i.e. $\nu^*_{0\rightarrow1}$ and $\nu^*_{1\rightarrow2}$) were the same as Figure 13.29 suggests then we could write the excitation energy as $2hc\,\nu^*_{0\rightarrow1}$. However, this is only approximately true because the vibrations, in general, are not *harmonic* as Figure 13.29 suggests but, in fact, they are *inharmonic* (c.f. Figure 13.33). As the result of inharmonicity:

$\nu^*_{1\rightarrow2} < \nu^*_{0\rightarrow1}$. Consequently, the excitation energy will be somewhat smaller than $2hc\nu^*_{0\rightarrow1}$:

$$\Delta E_{Overtone} = hc\,(\nu^*_{0\rightarrow1} + \nu^*_{1\rightarrow2}) < 2hc\nu^*_{0\rightarrow1} \qquad [130c]$$

Let us take a simple example formyl radical: H - C = O having a C - H and a C = O stretch. According to Table 13.3 the former of the two stretching modes occurs at $2800cm^{-1}$ and the latter at $1700cm^{-1}$.

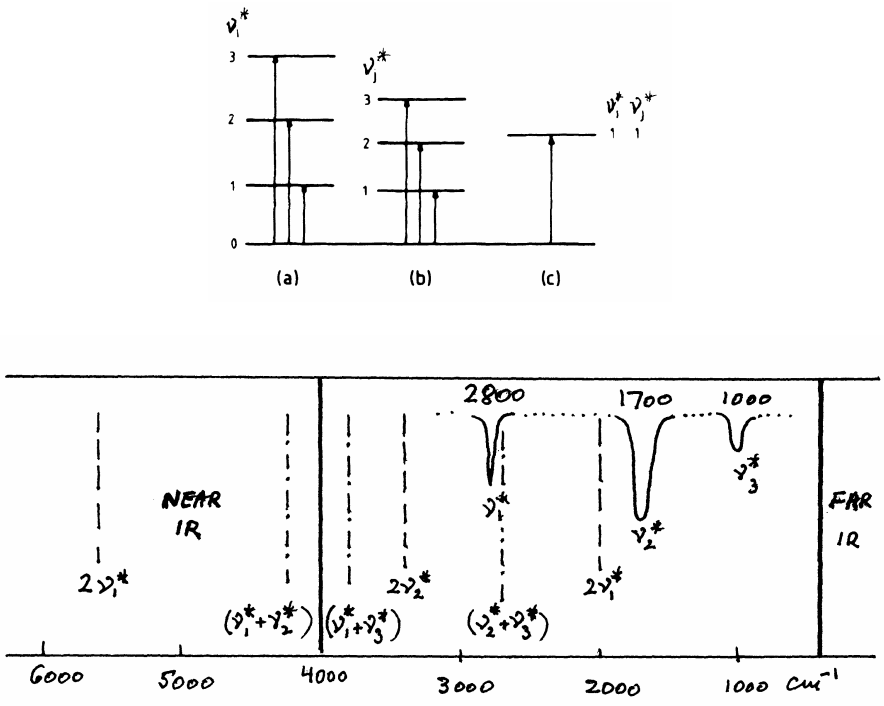

Figure 13.30 A schematic illustration of the C—H and C=O fundamental frequencies of the —CHO functionality.

The C=O stretch is always intense because the C=O functionality has a large dipole moment and it further increases during the stretch. In general, the intensities of the IR transitions depend on the change in dipole moment. If there is no change in dipole the intensity will be zero. If this is the case, we say that the vibration is infrared inactive.

Fortunately, the IR inactive frequencies can be observed in another branch of vibrational spectroscopy based on the Raman effect. In Raman spectroscopy a high-energy (i.e. short wavelength) photon is scattered, in an inelastic fashion, on the molecule. Due to the inelasticity of the scattering, some energy is lost (ΔE). The frequency change ($\Delta\nu$) of the incoming and outgoing photon falls in the range of vibrational excitation; [13.31]

$$\Delta E = h(\nu_{in} - \nu_{out}) = h\Delta\nu \qquad [13.31]$$

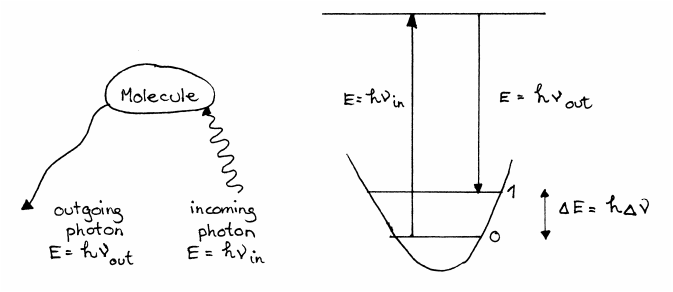

Figure 13.31 A schematic illustration of the Raman Effect.

The Raman intensity does not depend on the dipole change but on the change in polarizability (α). When a molecule is placed in a static electric field (ε), the molecule is *polarized*. This polarization (positively charged nuclei are attracted towards the negative pole etc.) is manifested in an *induced electric dipole moment* (μ)

$$\mu = \alpha\varepsilon \qquad [13.32]$$

The magnitude of polarizability (α) is different along the different directions and thus, it is characterized by an ellipsoid. Changes in α, along any of the principal axes of the ellipsoid, make the mode Raman active.

Certain vibrational modes are IR inactive and Raman active or vice versa depending on the symmetry of the molecule. This is illustrated for the acetylene molecule in Figure 13.32.

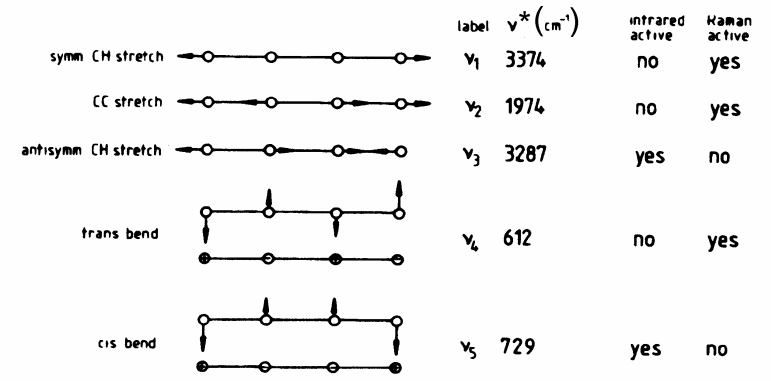

Figure 13.32 A schematic illustration of the normal modes of vibration of acetylene. Note that for linear molecules there are 3n-5 modes of motion. For acetylene, this gives 3 x 4 - 5 = 7 vibrations; ν_4 and ν_5 represent doubly degenerate bending along the x and along the y directions.

This alternating IR and Raman activity can only be observed in the case of highly symmetric molecules. For a general molecule, all frequencies may be both IR and Raman active. Consider, for example, crotonaldehyde [13.33], which has 11 atoms and therefore, 27 fundamental vibrations.

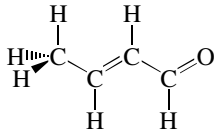

[13.33a]

3n - 6 = 3 x 11 - 6 = 27ved IR and Raman frequencies for crotonaldehyde are summarized in Table 13.4. Note that most of the frequencies were observed in both the IR and Raman spectra.

Table 13.4 IR and Raman fundamental vibration wavenumbers of crotonaldehyde.

Vibration	Approximate description	$\nu^*(cm^{-1})$	
		Infrared	Raman
In plane			
ν_1	CH antisymmetric stretch on C=C	3042	3032
ν_2	CH symmetric stretch on C=C	3002	3006
ν_3	CH_3 antisymmetric stretch	2944	2949
ν_4	CH_3 symmetric stretch	2916	2918
ν_5	CH stretch on CHO	2727	2732
ν_6	C=O stretch	1693	1682
ν_7	C=C stretch	1641	1641
ν_8	CH_3 antisymmetric deformation	1444	1445
ν_9	CH rock (in-plane bend) on CHO	1389	1393
ν_{10}	CH_3 symmetric deformation	1375	1380
ν_{11}	CH symmetric deformation on C=C	1305	1306
ν_{12}	CH antisymmetric deformation on C=C	1253	1252
ν_{13}	CH_3 in-plane rock	1075	1080
ν_{14}	C–CHO stretch	1042	1046
ν_{15}	C–CH_3 stretch	931	931
ν_{16}	CH_3–C=C bend	542	545
ν_{17}	C=C–C bend	459	464
ν_{18}	C–C=O bend	216	230
Out of plane			
ν_{19}	CH_3 antisymmetric stretch	2982	2976
ν_{20}	CH_3 antisymmetric deformation	1444	1445
ν_{20}	CH_3 antisymmetric deformation	1444	1445
ν_{21}	CH_3 rock	1146	1149
ν_{22}	CH antisymmetric[a)] deformation on C=C	966	-
ν_{23}	CH symmetric[a)] deformation on C=C	-	780
ν_{24}	CH wag (out-of-plane bend) on CHO	727	-
ν_{25}	CH_3 bend	297	300
ν_{26}	CH_3 torsion	173	-
ν_{27}	CHO torsion	121	-

a) To inversion of the two hydrogens through the center of the C = C bond.

The two sets of frequencies do differ from each other but the differences are rather minor.

In closing, we might mention that the vibrational spacings are not equidistant for realistic (i.e. inharmonic) vibration, as was the case for harmonic potentials (c.f. Figure 13.29). The consequence of inharmonicity is illustrated in Figure 13.33 for the H_2 molecule.

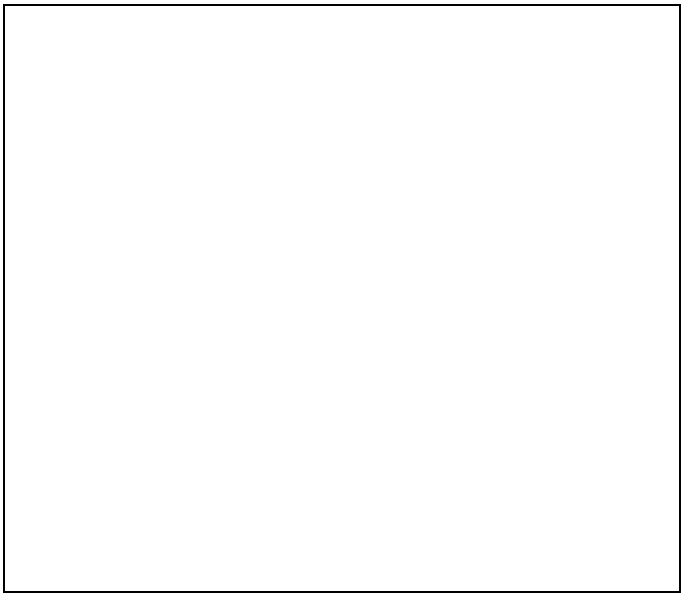

Figure 13.33 Potential energy curve and vibrational levels for H_2. The spacing of the vibrational levels are getting smaller and smaller and the discrete levels will become a continuum above the dissociation limit.

Examples from the literature

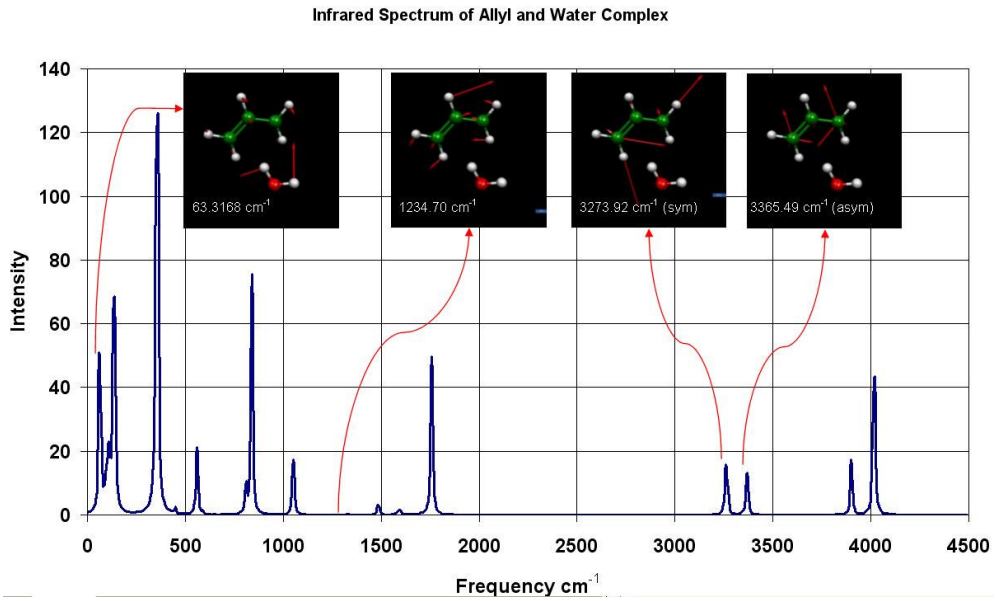

Hydrogen bondings in deoxynivalenol (DON) conformations

A density functional study

Introduction

Under normal circumstances, cereals can be infected by numerous types of pathogenic fungi. Some groups of these organisms can have a negative effect on the quality of foodstuff, and, which is more important, on the health of humans and animals as well. A major group of these dangerous pathogenic fungi is the *Fusarium* species. The dangerous effects of these species are due to their mycotoxin production. In 2002, the Scientific Committee on Food of the European Union formulated its opinion about the risk assessment of these toxins in nutrition [[1]].

The *Fusarium* species have a damaging effect on many types of cultivated plants and plants, in general. In humid weather conditions, they form a loose mycelium colony on the infected plant, which can be of yellow, off-white, pink or red in color. Through the ears of corn, the fungus gets easily on the seed. Considering their toxic effects, the most important cereal *Fusariums* are *Fusarium graminearum (***Figure 1***), F. culmorum, F. moniliforme,* and *F. sporotrichioides*. After the infection which takes place on the ploughed land, the production

of various toxins starts at that time and subsequently this production further increases under inappropriate storage conditions. The amount of toxins produced depends on the origin and the age of the fungi, as well as on the quality of the infected medium. These species of fungi produce several types of toxins having various effects.

The *fusario*toxins are classified according to their chemical structures, chromatographic properties and mechanisms of actions. The most important *fusario*toxins are: the Trichotecenes such as:

- Nivalenol (NIV)
- Deoxynivalenol (DON)
- T-2 toxin (acylated nivalenol)
- HT-2 toxin, etc.

According to literature data there exist more than 100 trichothecene type toxins in nature. The trichothecenes are tetracyclic sesquiterpenoid compounds with a 12,13-epoxy group. Those produced by Fusarium species belong to two categories according to functional groups. T-2 toxin and HT-2 toxin belong to **group A**, which is characterized by a functional group other than a carbonyl at C-8. Trichothecenes with a carbonyl group at C-8 belong to **group B** [2].

Deoxynivalenol (DON) is toxic and often found in foodstuffs, sometimes in high concentration. It has recently been of concern to international organizations and government food agencies. Deoxynivalenol (DON) and nivalenol belongs to the latter group. Other toxins such as Zearalenon and its derivatives, as well as Fumonisines are also of some importance.

The most prominent common effects of T-2 toxin, HT-2 toxin, DON and nivalenol (NIV) at the biochemical and cellular level are:

- strong inhibitory effect on the protein synthesis by binding to the ribosomes,
- inhibitory effect on RNA and DNA synthesis and
- toxic effects on cell membranes.

Another common effect is the induction of apoptosis particularly in lymphatic and haematopoietic tissue [3]. It appears that different trichothecenes differ in their capacity to inhibit protein synthesis, to activate the mitogen activated protein kinases (MAP kinases) and to induce apoptosis [4,5]. These mycotoxins also affect the human immune function [6]. It is not clear whether the toxins work *via* identical mechanisms at the biochemical and cellular level.

Scope

The deoxynivalenol molecule has been fully characterized as a tetracyclic sesquiterpene with seven stereo centers [7]. Its CA registration number is 51481-10-8 and its empirical formula is $C_{15}H_{20}O_6$. It's CA index name is Trichothec-9-en-8-one, 12,13-epoxy-3,7,15-trihydroxy-, (3α,7α)-(9CI). The compound is known by several other names, such as: Spiro [2,5-methano-1-benzoxepin-10,2'-oxirane], 4-Deoxynivalenol, 4-Desoxynivalenol, DON, Dehydronivalenol, NSC 269144, Vomitoxin.

In addition to two secondary and one primary alcoholic OH, two reactive functional groups are present in deoxynivalenol (**DON**): a conjugated ketone and an epoxide. At least one but maybe both of these two functionalities may be associated with the toxic activity of **DON**. Conjugated ketones may undergo Michael type additions (1) while non-symmetric epoxide rings may open readily after protonation (2).

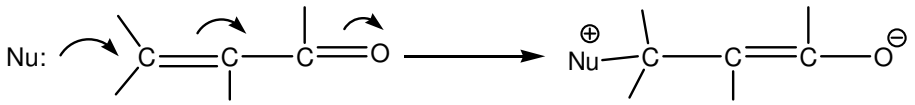

(1)

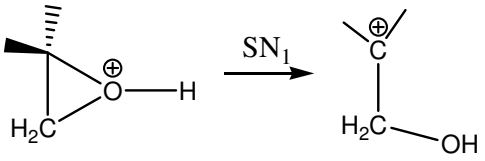

(2)

Clearly, there is *a priori* possibility for an SN_2 ring opening (3) but the molecule is rather crowded for an external nucleophile to execute such a ring opening mechanism.

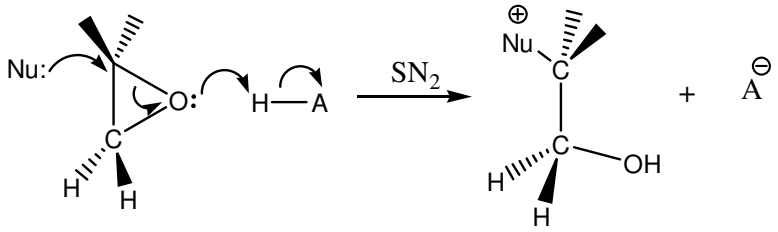

(3)

One of the purposes of the present paper is to see if the molecular conformation can enhance either one of the two possible modes of action via intramolecular hydrogen bonding.

Figure 2 shows the molecular structure of DON in 2D and 3D representations. A double hydrogen bonding system involves the oxygen of the conjugated ketone as the proton acceptor. These double H-bonds may reduce the π-electron density of the terminal carbon of the conjugate ketone and hence may enhance the Michael addition.

Rigid scans for the free rotors were used to characterize the potential energy hypersurface (**PEHS**) at the B3LYP/3-21G level of theory [[8],[9],[10]]. All minima of the **PEHS** were fully optimized at the same level of theory. The rotation about the bond between C^6 and C^{15} (see **Figure 2**) is coupled with the OH rotation about the bond C^{15}-O^{21}. The dihedral angles of the OH rotations are defined in the following way: χ_1=D(H-O-C^7-C^8), χ_2=D(C^6-C^{15}-O-H), χ_3=D(C^7-C^6-C^{15}-O^{21}), χ_4=D(H-O^{19}-C^3-C^2). The relative positions of both OH groups attached to C^2 and C^{15} are fixed due to strong hydrogen bonding. As a consequence, only eight of the possible 27 conformers were found. Two quasi identical conformations of the OH group attached to C^3 were also characterized, but their contribution to enhance the reactivity of the molecule is expected to be negligible.

To obtain more accurate relative energies, the selected conformers were re-optimized and the harmonic frequencies were calculated at the B3LYP/6-31G(d) level of theory. The ZPEs were scaled using the factor of 0.96 for B3LYP/6-31G(d) [[11]]. Each calculation was carried out using the Gaussian03 program package [[12]].

Results and discussion

Structural characteristics

The potential energy surface (PES), showing the variation of energy as a function of the orientation of the two OH groups, attached to C_7 and C_{15}, is shown in **Figure 3** as $E=f(\chi_1,\chi_2)$. This rigid PES reveals the existence of two minima E(**I**) = 0.00 and E(**II**) = 15.18 kJ/mol, when χ_3 was optimized to be about in the *anti* orientation. In addition to these two minima (**I** and **II**), six other structures (**III** – **VIII**) were located on the conformational PEHS. The characteristics of all these eight minima (**I** – **VIII**) are listed in **Table 1**.

The vibrational analysis of the global minimum revealed that the double hydrogen bond, involving the carbonyl oxygen as proton acceptor and the two OH groups attached to C^7 and C^{15} as proton donors, are indeed coupled.

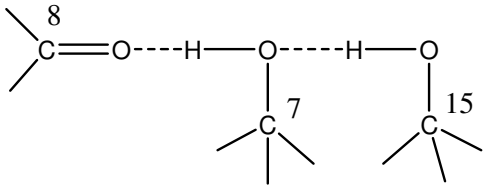

(4)

This is clearly illustrated by the vector diagram shown in **Figure 4** in terms of their coupled symmetric and asymmetric stretching vibrations. The molecular vibrational spectrum, for Conformation **I,** is also shown graphically in **Figure 4**. The possibility, whether this double hydrogen bonding does enhance the reactivity of the conjugated carbonyl, will be discussed in our subsequent publication. The epoxy group is not involved in internal hydrogen bonding. Consequently, if it is involved in a toxic biochemical reaction, its protic activation must come externally.

Energetic characteristics

Two structures (**I** and **IV**) were found with double hydrogen bonding as illustrated in (4) and **Figure 2B**. Structure **I** is the global minimum (ΔE=0.0 kJ/mol), depicted in its 3D form in **Figure 2B**. Structure **IV** is located within 3 kJ/mol above structure **I** on the conformational potential energy hypersurface. There is a group of conformers (**III** and **VI**) in the vicinity of 9 kJ/mol on the stability scale, while the other structures (**V**, **VII** and **VIII**) are about 12 kJ/mol above the global minimum.

Conclusions

Conformation **I**, a double H-bonded structure of deoxynivalenol, turned out to be the global minimum of the total of eight conformations optimized at the B3LYP/6-31G(d) level of theory.

In the two double H-bonded structures of deoxynivalenol (**I** and **IV**) the two OH stretching frequencies were coupled to symmetric and antisymmetric stretches. The second double H-bonded structure (**IV**) has a higher energy (lower H-bond strength); as a consequence the coupling of the two stretching frequencies was not as strong as in case of structure **I**. These two structures have the lowest total entropy among the eight conformations, so the appearance of an extra hydrogen bond lowers the entropy of the molecule.

Acknowledgements

The authors are grateful to the Hungarian Scientific Research Fund (OTKA T046861 and F037648).

Table 1.
Geometrical characteristics of DON in its eight conformations optimized at the B3LYP/6-31G(d) level of theory

Structures		Dihedral Angles				Energy values		Hydrogen bond lengths (Å)		
Code	Conformation	χ_1	χ_2	χ_3	χ_4	E (Hartree)	ΔE (kJ/mol)	$C^8O....HOC^7$	$C^7-O....HOC^{15}$	Total Entropy (J/(mol K))
I	$[sg^+g^-]g^+$	-18.8	38.3	-61.3	51.4	**-1034.87148**	0	1.94	1.92	136.23
II	$[sag^-]g^+$	61.0	163.0	-43.7	46.1	-1034.86399	19.66	2.60[1]	---	138.55
III	$[sg^+g^+]g^+$	-11.3	67.4	53.7	47.1	-1034.868092	8.89	1.97	---	137.53
IV	$[sg^-g^+]g^+$	-26.3	-63.0	14.0	47.4	-1034.870432	2.75	1.97	2.09	137.13
V	$[sag^+]g^+$	-12.6	-156.7	61.8	-1.2[2]	-1034.866109	14.10	1.95	---	137.94
VI	$[sg^+a]g^+$	-12.6	83.4	179.1	46.5	-1034.86734	10.86	1.96	---	138.195
VII	$[saa]g^+$	-14.1	176.3	173.5	47.9	-1034.867074	11.57	1.96	---	139.24
VIII	$[sg^-a]g^+$	-13.7	-74.0	177.2	50.2	-1034.866879	12.08	1.97	---	138.61

[1] A stronger hydrogen bond was found ($C^{15}O....HOC^7$), with the H-bond length of 2.03 Å
[2] The conformer having the χ_4 dihedral angle in gauche conformation was not found on the potential energy hypersurface

Figure captions

Figure 1. *Fusarium graminearum* in 250 x magnification

Figure 2. Molecular Structure of Deoxynivalenol (DON)

A. 2D Structure with numbering system and designation of absolute configurations (in terms of R and S) of all chiral centers.

B. 3D Structure with numbering system showing the double hydrogen bounded system in which the oxygen of the unsaturated ketone is the proton acceptor. The accessibility of an incoming nucleophile to C^{10} is clearly seen. Also the epoxy oxygen is not hindered to protonation.

Figure 3. Potential Energy Surface (PES) obtained at the B3LYP/6-31G level of theory showing potential energy as a function of rotation about the C^7-OH and C^{15}-OH bonds. Torsional angle χ_3 was optimized at about *anti* orientation.

Figure 4. Calculated vibrational spectrum and vectorial representation of normal modes of motion associated with the coupled symmetric and antisymmetric stretching vibrations of the two double hydrogen bonded systems of Deoxynivalenol (DON) involving:

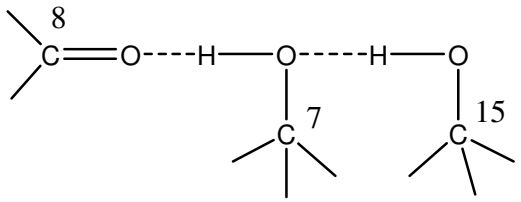

Figure 5. Geometrically faithful 3D representation of optimized conformers of DON

Figure 1

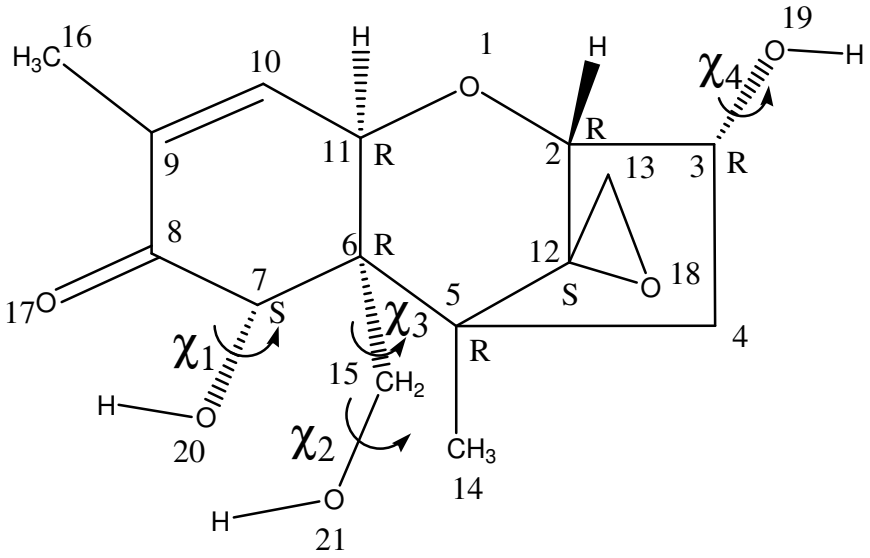
H3C
16
10
H
1
H
19
O
H
χ4
9
11
R
2
R
13
3
R
8
6
R
12
7
5
S
S
O
18
17O
χ1
χ3
R
4
15
CH2
H
O
20
χ2
CH3
14
H
O
21

A

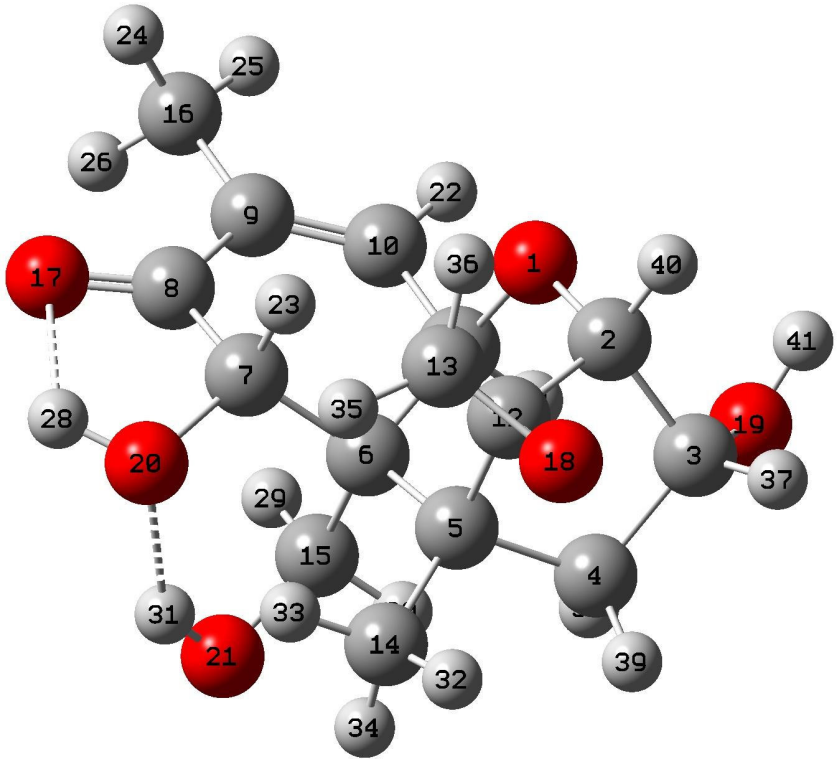
24
25
16
26
9
22
10
17
8
36
1
40
23
2
41
7
13
28
35
19
20
6
18
3
37
29
5
15
4
31
33
14
21
39
32
34

B

Figure 2

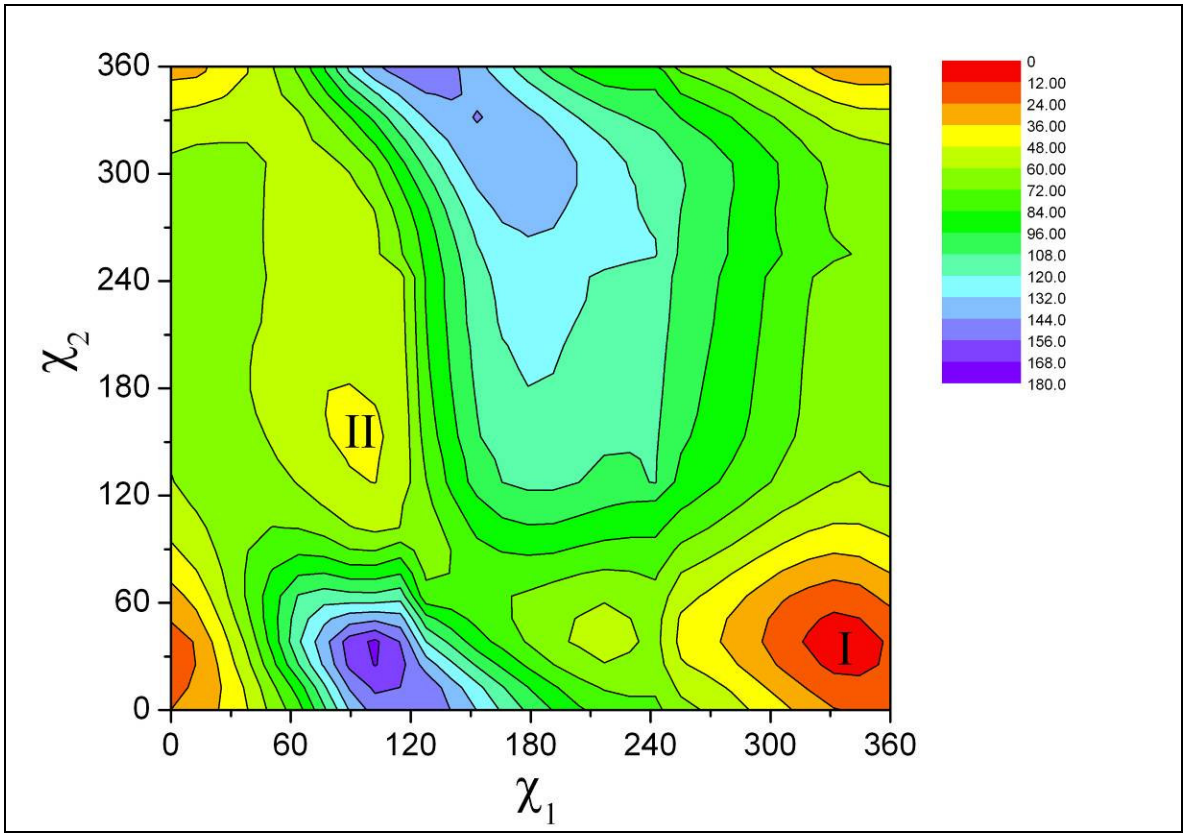
360
300
240
180
120
60
0
χ2
0
60
120
180
240
300
360
χ1
II
I
0
12.00
24.00
36.00
48.00
60.00
72.00
84.00
96.00
108.0
120.0
132.0
144.0
156.0
168.0
180.0

Figure 3

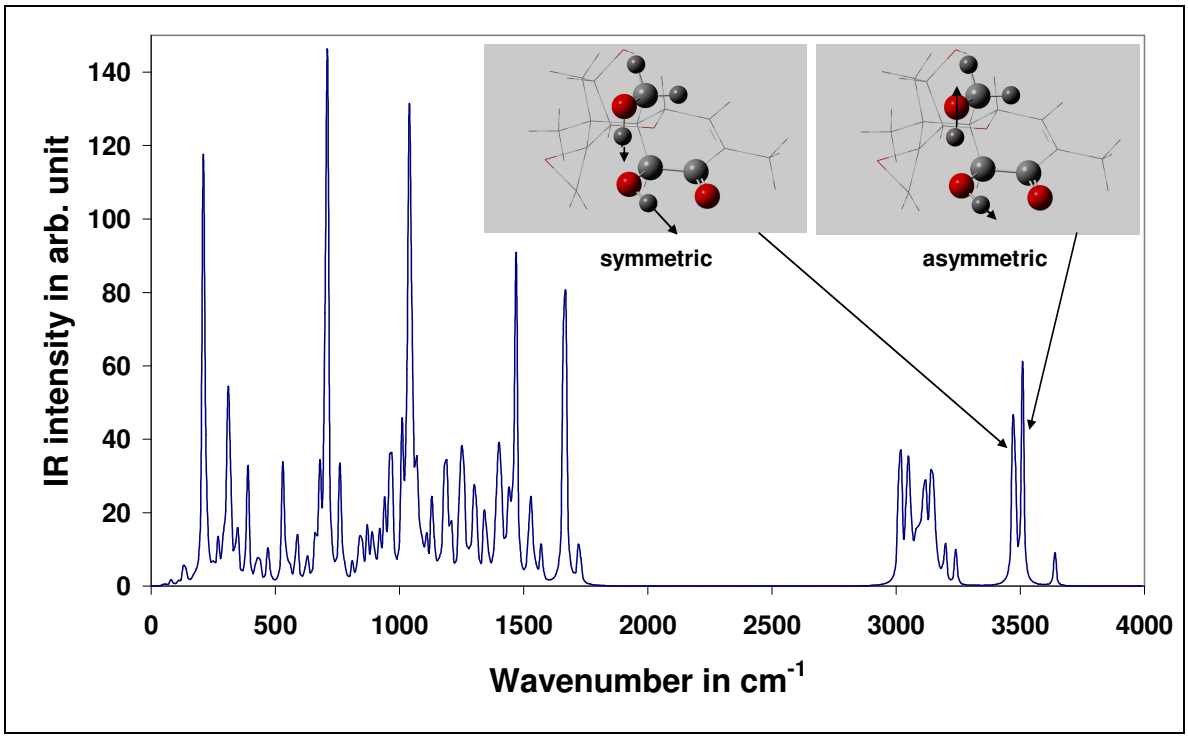
IR intensity in arb. unit
140
120
100
80
60
40
20
0
0
500
1000
1500
2000
2500
3000
3500
4000
Wavenumber in cm-1
symmetric
asymmetric

a.

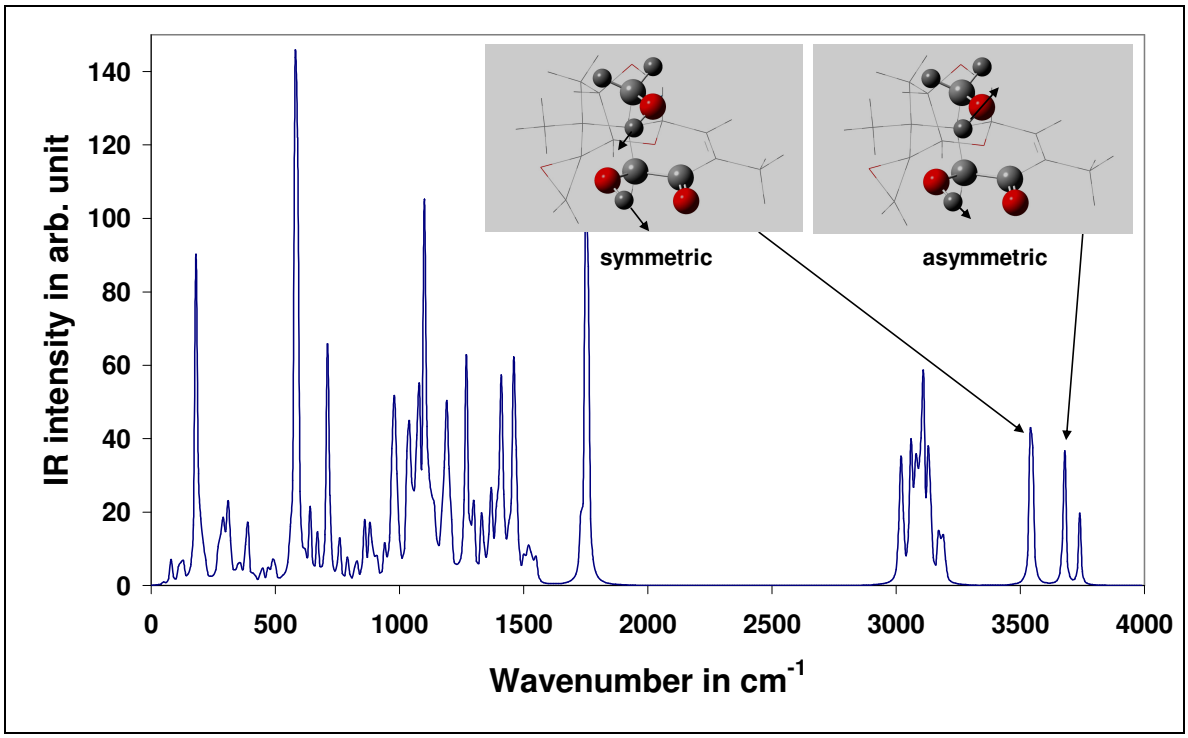
IR intensity in arb. unit
140
120
100
80
60
40
20
0
0
500
1000
1500
2000
2500
3000
3500
4000
Wavenumber in cm-1
symmetric
asymmetric

b.

Figure 4

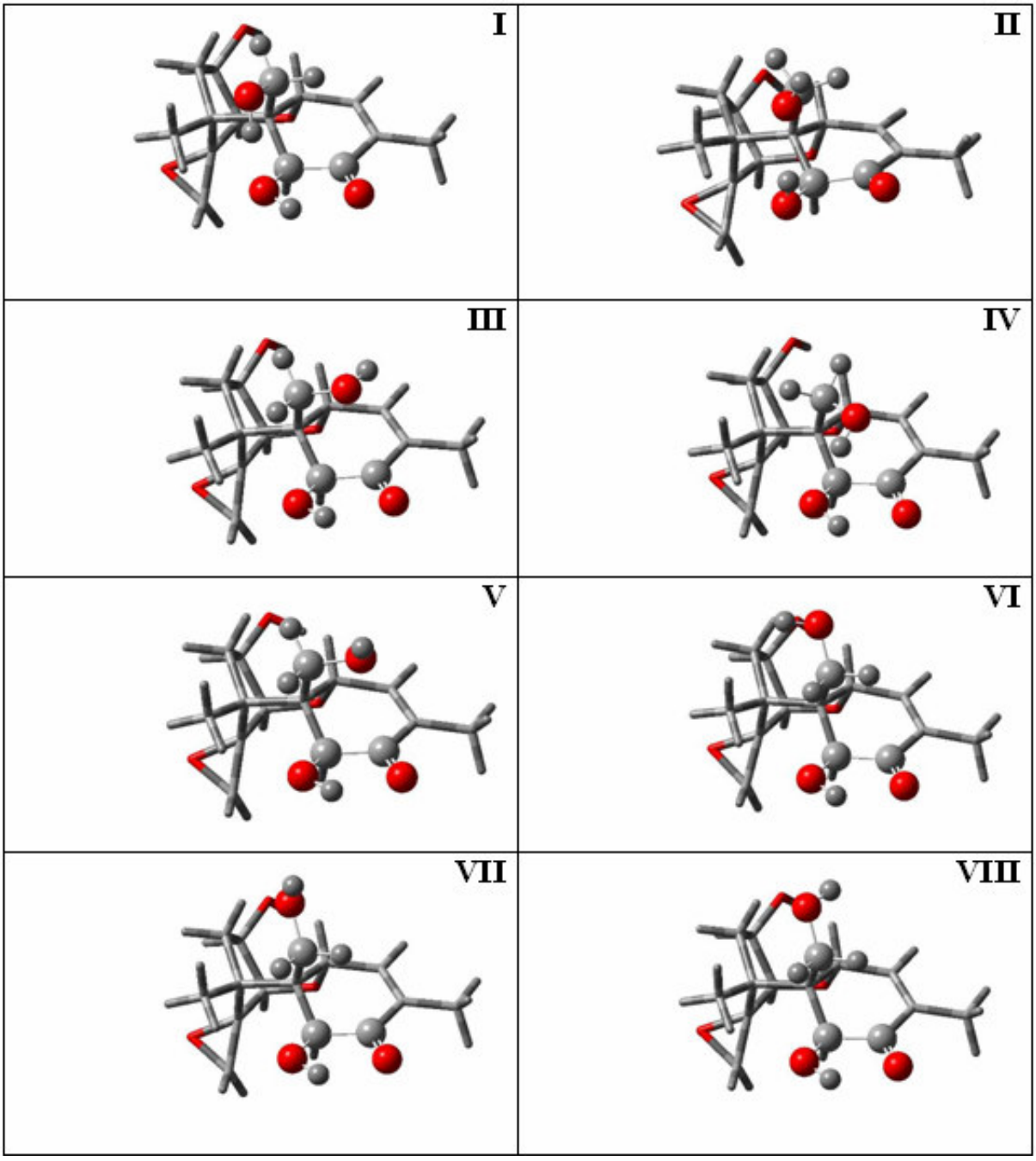

Figure 5

Vibrational Analysis in Gaussian

2.1 Mass weight the Hessian and diagonalize

We start with the Hessian matrix fCART, which holds the second partial derivatives of the potential V with respect to displacement of the atoms in cartesian coordinates (CART):

$$f_{CARTij} = \left(\frac{\partial^2 V}{\partial \xi_i \partial \xi_j} \right)_0 \qquad (1)$$

This is a 3N x 3N matrix (N is the number of atoms), where $\xi_1;\xi_2;\ \xi_3$ …3N are used for the displacements in cartesian coordinates, $\Delta x_1;\ \Delta y_1;\ \Delta z_1;\quad \Delta z_N$. The $()_0$ refers to the fact that the derivatives are taken at the equilibrium positions of the atoms, and that the first derivatives are zero.

The first thing that Gaussian does with these force constants is to convert them to mass weighted cartesian coordinates (MWC).

$$f_{MWCi,j} = \frac{f_{CARTij}}{\sqrt{m_i m_j}} = \left(\frac{\partial^2 V}{\partial q_i \partial q_j} \right)_0 \qquad (2)$$

where $q_1 = \sqrt{m_1}\xi_1 = \sqrt{m_1}\Delta x_1$ and so on, are the mass weighted cartesian coordinates.

A copy of $\mathbf{f}_{MWC}$ is diagonalized, yielding a set of 3N eigenvectors and 3N eigenvalues. The eigenvectors, which are the normal modes, are discarded; they will be calculated again after the rotation and translation modes are separated out. The roots of the eigenvalues are the fundamental frequencies of the molecule. Gaussian converts them to cm^{-1}, then prints out the 3N (up to 9) lowest. The output for water HF/3-21G* looks like this:

Full mass-weighted force constant matrix:
Low frequencies --- -0.0008 0.0003 0.0013 40.6275 59.3808 66.4408
Low frequencies --- 1799.1892 3809.4604 3943.3536

In general, the frequencies for for rotation and translation modes should be close to zero. If you have optimized to a transition state, or to a higher order saddle point, then there will be some negative frequencies which may be listed before the \zero frequency" modes. (Freqencies which are printed out as negative are really imaginary; the minus sign is simply a ag to indicate that this is an imaginary frequency.) There is a discussion about how close to zero is close enough, and what to do if you are not close enough in Section 4 of this paper.

You should compare the lowest real frequencies list in this part of the output with the corresponding frequencies later in the output. The later frequencies are calculated after projecting out

the translational and rotational modes. If the corresponding frequencies in both places are not the same, then this is an indication that these modes are contaminated by the rotational and translational modes.

2.2 Determine the principal axes of inertia

The next step is to translate the center of mass to the origin, and determine the moments and products of inertia, with the goal of finding the matrix that diagonalizes the moment of inertia tensor. Using this matrix we can find the vectors corresponding to the rotations and translations. Once these vectors are known, we know that the rest of the normal modes are vibrations, so we can distinguish low frequency vibrational modes from rotational and translational modes.

The center of mass ($\mathbf{R}_{COM}$) is found in the usual way:

$$R_{COM} = \frac{\sum_{\alpha} m_\alpha r_\alpha}{\sum_{\alpha} m_\alpha} \tag{3}$$

where the sums are over the atoms, α. The origin is then shifted to the center of mass $r_{COM\alpha} = r_\alpha - \mathbf{R}_{COM}$. Next we have to calculate the moments of inertia (the diagonal elements) and the products of inertia (off diagonal elements) of the moment of inertia tensor (**I**).

$$I = \begin{pmatrix} I_{xx} & I_{xy} & I_{xz} \\ I_{yx} & I_{yy} & I_{yz} \\ I_{yz} & I_{zy} & I_{zz} \end{pmatrix} = \begin{pmatrix} \sum_\alpha m_\alpha (y_\alpha^2 + z_\alpha^2) & -\sum_\alpha m_\alpha (x_\alpha y_\alpha) & -\sum_\alpha m_\alpha (x_\alpha z_\alpha) \\ -\sum_\alpha m_\alpha (y_\alpha x_\alpha) & \sum_\alpha m_\alpha (x_\alpha^2 + z_\alpha^2) & -\sum_\alpha m_\alpha (y_\alpha z_\alpha) \\ -\sum_\alpha m_\alpha (z_\alpha x_\alpha) & -\sum_\alpha m_\alpha (z_\alpha y_\alpha) & \sum_\alpha m_\alpha (x_\alpha^2 + y_\alpha^2) \end{pmatrix} \tag{4}$$

This symmetric matrix is diagonalized, yielding the principal moments (the eigenvalues **I**') and a 3_3 matrix (**X**), which is made up of the normalized eigenvectors of **I**. The eigenvectors of the moment of inertia tensor are used to generate the vectors corresponding to translation and in_nitesimal rotation of the molecule in the next step.

2.3 Generate coordinates in the rotating and translating frame

The main goal in this section is to generate the transformation **D** from mass weighted Cartesian coordinates to a set of 3N coordinates where rotation and translation of the molecule are separated out, leaving 3N - 6 or 3N – 5 modes for vibrational analysis. The rest of this section describes how the Sayvetz conditions are used to generate the translation and rotation vectors.

The three vectors (**D1, D2, D3**) of length 3N corresponding to translation are trivial to generate in cartesian coordinates. They are just $\sqrt{m_i}$ times the corresponding coordinate axis. For example, for water (using $m_H = 1$ and $m_O = 16$) the translational vectors are:

$$\mathbf{D1} = (1; 0; 0; 4; 0; 0; 1; 0; 0)^t$$

$$\mathbf{D2} = (0; 1; 0; 0; 4; 0; 0; 1; 0)^t$$

$$\mathbf{D3} = (0; 0; 1; 0; 0; 4; 0; 0; 1)^t$$

Generating vectors corresponding to rotational motion of the atoms in cartesian coordinates is a bit more complicated. The vectors for these are defined this way:

$$D_{4j;i} = ((P_y)_i X_{j;3} - (P_z)_i X_{j;2})/\sqrt{m_i}$$

$$D_{5j;i} = ((P_z)_i X_{j;1} - (P_x)_i X_{j;3})/\sqrt{m_i}$$

$$D_{6j;i} = ((P_x)_i X_{j;2} - (P_y)_i X_{j;1})/\sqrt{m_i}$$

(5)

where j = x; y; z; i is over all atoms and P is the dot product of **R** (the coordinates of the atoms with respect to the center of mass) and the corresponding row of **X**, the matrix used to diagonalize the moment of inertia tensor **I**.

The next step is to normalize these vectors. If the molecule is linear (or is a single atoms), any vectors which do not correspond to translational or rotational normal modes are removed. The scalar product is taken of each vector with itself. If it is zero (or very close to it), then that vector is not an actual normal mode and it is eliminated. (If the scalar product is zero, this mode will disappear when the transformation from mass weighted to internal coordinates is done, in Equation 6.) Otherwise, the vector is normalized using the reciprocal square root of the scalar product. Gaussian then checks to see that the number of rotational and translational modes is what's expected for the molecule, three for atoms, _ve for linear molecules and six for all others. If this is not the case, Gaussian prints an error message and aborts.

A Schmidt orthogonalization is used to generate N_{vib} = 3N - 6 (or 3N - 5) remaining vectors, which are orthogonal to the five or six rotational and translational vectors. The result is a transformation matrix **D** which transforms from mass weighted cartesian coordinates **q** to internal coordinates **S = Dq**, where rotation and translation have been separated out.

2.4 Transform the Hessian to internal coordinates and diagonalize

Now that we have coordinates in the rotating and translating frame, we need to transform the Hessian, $\mathbf{f}_{MWC}$ (still in mass weighted cartesian coordinates), to these new internal coordinates (INT). Only the N_{vib} coordinates corresponding to internal coordinates will be diagonalized, although the full 3N coordinates are used to transform the Hessian. The transformation is straightforward:

$$\mathbf{f}_{INT} = \mathbf{D}^{\dagger}\mathbf{f}_{MWC}\mathbf{D} \qquad (6)$$

The N_{vib} x N_{vib} submatrix of $\mathbf{f}_{INT}$, which represents the force constants internal coordinates, is diagonalized yielding N_{vib} eigenvalues $\lambda = 4\pi^2\nu^2$ and N_{vib} eigenvectors. If we call the transformation matrix composed of the eigenvectors **L**, then we have

$$\mathbf{L}^{\dagger}\mathbf{f}_{INT}\mathbf{L}=\mathbf{\Lambda} \tag{7}$$

where $\mathbf{\Lambda}$ is the diagonal matrix with eigenvalues λi.

2.5 Calculate the frequencies

At this point, the eigenvalues need to be converted frequencies in units of reciprocal centimeters. First we change from frequencies (ν_i) to wave numbers (ν^*_i), via the relationship $\nu_i = \nu^*_i c$, where c is the speed of light. Solving $\lambda = 4\pi^2\nu^{*2} c^2$ for ν^*_i we get

$$\nu_i^* = \sqrt{\frac{\lambda_i}{4\pi^2 c^2}} \tag{8}$$

The rest is simply applying the appropriate conversion factors: from a single molecule to a mole, from hartrees to joules, and from atomic mass units to kilograms. For negative eigenvalues, we calculate ν^*_i using the absolute value of λ_i, then multiply by -1 to make the frequency negative (which flags it as imaginary). After this conversion, the frequencies are ready to be printed out.

2.6 Calculate reduced mass, force constants and cartesian displacements

All the pieces are now in place to calculate the reduced mass, force constants and Cartesian displacements. Combining Equation 6 and Equation 7, we arrive at

$$\mathbf{L}^{\dagger}\mathbf{D}^{\dagger}\mathbf{f}_{MWC}\mathbf{DL}=\mathbf{\Lambda}=\mathbf{l}_{MWC}{}^{\dagger}\mathbf{f}_{MWC}\,\mathbf{l}_{MWC} \tag{9}$$

where $\mathbf{l} = \mathbf{DL}$ is the matrix needed to diagonalize $\mathbf{f}_{MWC}$. Actually, $\mathbf{l}_{MWC}$ is never calculated directly in Gaussian. Instead, $\mathbf{l}_{CART} = \mathbf{MDL}$ is calculated, where $\mathbf{M}$ is a diagonal matrix defined by:

$$M_{i,j} = \frac{1}{\sqrt{m_i}} \tag{10}$$

and i runs over the x, y, and z coordinates for every atom. The individual elements of $\mathbf{l}_{CART}$ are given by:

$$l_{CARTk,i} = \sum_{j}^{3N}\left(\frac{D_{k,j}L_{j,i}}{\sqrt{m_j}}\right) \tag{11}$$

The column vectors of these elements, which are the normal modes in cartesian coordinates, are used in several ways. First of all, once normalized by the procedure described below, they are the displacements in cartesian coordinates. Secondly, they are useful for calculating a number of spectroscopic properties, including IR intensities, Raman activies, depolarizations and dipole and rotational strengths for VCD.

Normalization is a relatively straight forward process. Before it is printed out, each of the 3N elements of l_{CARTi} is scaled by normalization factor $\mathcal{N}_i$, for that particular vibrational mode. The normalization is defined by:

$$\mathcal{N}_i = \sqrt{\left(\sum_k^{3N} l^2_{CARTk,i}\right)^{-1}} \qquad (12)$$

The reduced mass _i for the vibrational mode is calculated in a similar fashion:

$$\mu i = \left(\sum_k^{3N} l^2_{CARTk,i}\right)^{-1} = \left(\sum_k^{3N}\left(\frac{l_{MWCk,i}}{\sqrt{m_j}}\right)^2\right)^{-1} = \left(\sum_k^{3N}\left(\frac{l^2_{MWCk,i}}{m_j}\right)\right)^{-1} = \mathcal{N}_i^2 \qquad (13)$$

Note that since **D** is orthonormal, and we can (and do) choose **L** to be orthonormal, then **l** is orthonormal as well. (Since $\mathbf{D}^\dagger\mathbf{D} = 1$;$\mathbf{L}^\dagger\mathbf{L} = 1$ then $\mathbf{l}^\dagger\mathbf{l} = \mathbf{(DL)}^\dagger\mathbf{DL} = \mathbf{L}^\dagger\mathbf{D}^\dagger\mathbf{DL} = \mathbf{L}^\dagger\mathbf{1L} = \mathbf{1}$).

We now have enough information to explain the di_erence between the reduced mass Gaussian prints out, and the one calculated using the formula usually used for diatomics:

$$\frac{1}{\mu} = \frac{1}{m_1} + \frac{1}{m_2} \qquad (14)$$

The difference is in the numerator of each term in the summation. Gaussian uses $l^2_{MWCk,i}$ rather than 1. Using the elements of $\mathbf{l}_{MWC}$ yields the consistent results for polyatomic cases, and automatically takes symmtery into consideration. Simply extending the formula from Equation 14 to $\frac{1}{\mu} = \sum_i^{atoms} \frac{1}{m_i}$ would (incorrectly) yield the same reduced mass for every mode of a polyatomic molecule.

The effect of using the elements of $\mathbf{l}_{MWC}$ in the numerator is to make the unit length of the coordinate system Gaussian uses be the normalized cartesian displacement. In other words, in the coordinate system that Gaussian uses, the sum of the squares of the Cartesian displacements is 1. (You can check this in the output). In the more common coordinate system for diatomics, the unit length is a unit change in internuclear distance from the equilibrium value.

One of the consequences of using this coordinate system is that force constants which you think should be equal are not. A simple example is H_2 versus HD. Since the Hessian depends only on the electronic part of the Hamiltonian, you would expect the force constants to be the same for these to molecules. In fact, the force constant Gaussian prints out is different. The different masses of the atoms leads to a different set of Sayvetz conditions, which in turn, change the internal coordinate system the force constants are transformed to, and ultimately the resulting force constant.

The coordinates used to calculate the force constants, the reduced mass and the Cartesian displacements are all internally consistent. The force constants k_i are given by $k_i = 4\pi^2\nu^{*2}\,\mu_i$ since $\nu^* = \frac{1}{2\pi}\sqrt{\frac{k_i}{\mu_i}}$ The force constants are converted from atomic units to millidyne/angstrom.

3 Summary

To summarize, the steps Gaussian uses to perform vibrational analysis are:

1. Mass weight the Hessian

$$f_{MWCij} = \frac{f_{CARTij}}{\sqrt{m_i m_j}}$$

2. Determine the principal axes of inertia

$$I' = X^{\dagger} I X$$

3. Generate coordinates in the rotating and translating frame

$$S = Dq$$

4. Transform the Hessian to internal coordinates and diagonalize

$$\mathbf{f}_{INT} = \mathbf{D}^{\dagger}\mathbf{f}_{MWC}\mathbf{D}$$

$$L^{\dagger} f_{INT} L = \mathbf{\Lambda}$$

5. Calculate the frequencies

$$\nu_i^* = \sqrt{\frac{\lambda_i}{4\pi^2 c^2}}$$

6. Calculate reduced mass, force constants and cartesian displacements

$$\mu i = \left(\sum_{k}^{3N} l_{CARTk,i}^2 \right)^{-1}$$

$$k_i = 4\pi^2 \nu^{*2} \mu_i$$

$$l_{CART} = \mathbf{MDL}$$

Criteria	Low frequencies					
Opt	-0,0008	0,0003	0,0013	40,6275	59,3808	66,4408
Opt=Tight	0,0011	0,0013	0,0015	4,1908	-6,8779	12,4224
Opt=VeryTight	-0,0011	0,0014	0,0015	-0,9207	-1,1831	-1,6023

Table 1: The effect of optimization criteria on the low frequencies of water using HF/3-21G*.The frequencies are sorted by increasing absolute value, so that it's easier to distinguish rotational modes from vibrational modes.

4 A note about low frequencies

You'll find that the frequencies for the translations are almost always extremely close to zero. The frequencies for rotations are quite a bit larger. So, how “close to zero" is close enough? For most methods (HF, MP2, etc.), you'd like the rotational frequencies to be around 10 wavenumbers or less. For methods which use numerical integration, like DFT, the frequencies should be less than a few tens of wavenumbers, say 50 or so.

If the frequencies for rotations are not close to zero, it may be a signal that you need to do a tighter optimization. There are a couple of ways to accomplish this. For most methods, you can use Opt=Tight or Opt=Verytight on the route card to specify that you'd like to usetighter convergence criteria. For DFT, you may also need to specify Int=Ultra_ne, which uses a more accurate numerical integration grid.

As an example, I reran the water HF/3-21G* calculation above, with both Opt=Tight and Opt=VeryTight. You can see in Table 1 that the rotational frequencies are an order of magnitude better for Opt=Tight than they were for just Opt. Using Opt=Verytight makes them even better. This raises the question of whether the you need to use tighter convergence. The answer is: it depends { di_erent users will be interested in di_erent results. There is a trade o_ between accuracy and speed. Using Opt=Tight or Int=Ultra_ne makes the calculation take longer in addition to making the results more accurate. The default convergence criteria are set to give an accuracy good enough for most purposes without spending time to converge the results beyond this accuracy. You may _nd that you need to use the tighter criteria to compare to spectroscopic values, or to resolve a strucutre witha particularly at potential energy surface.

In the water frequency calculation above, using tighter convergence criteria makes almost no di_erence in terms of energy or bond lengths, as Table 2 demonstrates. The energy is converged to less then 1 microHartree, and the OH bond length is converged to 0.0002 angstroms. Tightening up the convergence criteria is useful for getting a couple of extradigits of precision in the symmetric stretch frequency.

You can also see that the _nal geometry parameters obtained with the default optimization criteria depend somewhat on the initial starting geometry. Using Opt=VeryTight all but eliminates these di_erences. I've included the starting geometries in Table 3, for those who wish to reproduce these results. (Using the default convergence criteria may give somewhat di_erent results than those I've shown if you use a di_erent machine, or even the same machine using di_erent libraries or a di_erent version of the compiler).

With DFT, Opt=VeryTight alone is not necessarily enough to converge the geometry to

Criteria	Start Geom	Energy	R_{OH}	A_{HOH}	Bend	Symmetric Strech	Antisymm. Sterch
Opt	A	-75:5859596012	0:9669	107:7241	1799:1892	3809:4604	3943:3536
Opt	B	-75:5859596488	0:9665	107:6348	1799:5957	3814:2216	3947:2011
Opt=Tight	A	-75:5859597578	0:9667	107:6784	1799:3335	3812:3499	3945:7723
Opt=Tight	B	-75:5859597580	0:9667	107:6811	1799:3156	3812:2440	3945:6938
Opt=VeryTight	A	-75:5859597582	0:9667	107:6818	1799:2877	3812:3779	3945:8339
Opt=VeryTight	B	-75:5859597582	0:9667	107:6820	1799:2854	3812:3847	3945:8418

Table 2: The default optimization settings yield results accurate enough for most purposes.Tighter optimizations make almost no di_erence for this HF/3-21G* frequency calculation on water.

Geometry A	Geometry B
O H,1,R2 H,1,R2,2,A3 R2=0.96 A3=109,47122063	O H,1,R2 H,1,R2,2,A3 R2=1.0 A3=109.5

Table 3: Initial geometries for water optimization calculations. Geometry A was producedby Geom=ModelA. Geometry B is a slightly modi_ed version of Geometry A.

the point where the low frequencies are as close to zero as you would like. To demonstrate this, I have run B3LYP/3-21G* optimizations on water, starting with geometry B from Table 3, with Opt, Opt=Tight and Opt=VeryTight. The results are in Table 4. The low frequencies from these two jobs hardly change, and in fact get worse for the Tight and VeryTight optimizations.

Given the straight forward convergence seen with Hartree-Fock theory, this might not seem to make sense. However, it does make sense if you recall that DFT is done using a numerical integration on a grid of points. The accuracy of the default grid is not highenough for computing low frequency modes very precisely. The solution is to use a morenumerically accurate grid. The tighter the optimzation criteria, the more accurate the gridneeds to be. As you can see in Table 4, increasinfg the convergence criteria from Tight to VeryTight without increasing the numerical accuracy of the grid yields no improvement in the low frequencies. For Opt=Tight, we recommend using the Ultra_ne grid. This is a good combination to use for systems with hindered rotors, or if exact conformation is of concern. If still more accuracy is necessary, then an unpruned 199974 grid can be used with Opt=VeryTight. Again, the higher accuracy comes at a higher cost in terms of CPU time.The VeryTight optimization with a 199974 grid is very expensive, even for medium sized molecules. The default grids are accurate enough for most purposes.

Criteria	Grid	Low frequencies
Opt	FineGrid	0,0005 -0,0011 0,0011 16,5776 17,8265 -38,2354
Opt=Tight	FineGrid	-0,0011 -0,0011 0,0005 25,8979 -29,0202 37,0170
Opt=VeryTight	FineGrid	-0,0006 -0,0007 -0,0008 25,8977 -29,0203 37,0168
Opt=Tight	UltraFine	0,0012 0,0022 0,0024 -1,5386 -4,8182 -9,0313
Opt=VeryTight	UltraFine	0,0012 0,0022 0,0024 -1,5386 -4,8182 -9,0313
Opt=VeryTight	Gird=199974	-0,0004 0,0010 0,0011 -4,8721 -5,3561 -6,3672

Table 4: The e-ect of grid size on the low frequencies from B3LYP/3-21G* on water with Opt, Opt=Tight and Opt=VeryTight. More accurate grids are necessary for a truly converged optimization. The frequencies are sorted by increasing absolute value, so that it's easier to distinguish rotational modes from vibrational modes.

[1] Scientific Committee on Food (2002). Opinion of the Scientific Committee on Food on Fusarium toxins. Part 6: Group evaluation of T-2 toxin, HT-2 toxin, nivalenol and Deoxynivalenol (expressed on 26 February 2002)
[2] Eriksen G.S., Alexander J. (eds.) (1998). Fusarium toxins in cereals – a risk assessment. Nordic Council of Ministers, Tema Nord 1998, 502, Copenhagen
[3] Scientific Committee on Food (1999). Opinion on Fusarium Toxins - Part 1: Deoxynivalenol (DON) (expressed on 2 December 1999).
[4] Shifrin V.L., Anderson P. (1999). Trichothecene mycotoxins trigger ribotoxic stress response that activates c-Jun N-terminal kinase and p38 mitogen-activated protein kinase and induces apoptosis. J. Biol. Chem., 274, 13985-13992
[5] Yang, G-H., Jarvis, B.B., Chung, Y-J., Pestka, J.J. (2000) Apoptosis induction by satratoxins and other trichothecene mycotoxins: Relationship to ERK, p38 MAPK, and SAPK/JNK activation. Toxicol. Appl. Pharmacol., 164, 149-160
[6] L. Berek, I. Petri, A. Mesterhazi, J. Teren, J. Molnar; Toxicology in vitro, 15, 25-30 (2001)
[7] Bruce B. Jarvis, Dorothy Bruns Mazzocchi, Herman L. Ammon, Eugene P. Mazzola, Judith L. Flippen-Anderson, Richard D. Gilardi, Clifford F. George; J. Org. Chem.; 1990; 55(11); 3660-3662
[8] S. H. Vosko, L. Wilk, and M. Nusair, *Can. J. Phys* . **58**, 1200 (1980)
[9] C. Lee, W. Yang, and R. G. Parr, *Phys. Rev. B* **37**, 785 (1988)
[10] B. Miehlich, A. Savin, H. Stoll, and H. Preuss, *Chem. Phys. Lett.* **157**, 200 (1989)
[11] Scott A. P., Radom, L. *J. Phys. Chem* **1996**, *100,* 16502-16513
[12] *Gaussian 03, Revision B.01,* M. J. Frisch, G. W. Trucks, H. B. Schlegel, G. E. Scuseria, M. A. Robb, J. R. Cheeseman, J. A. Montgomery, Jr., T. Vreven, K. N. Kudin, J. C. Burant, J. M. Millam, S. S. Iyengar, J. Tomasi, V. Barone, B. Mennucci, M. Cossi, G. Scalmani, N. Rega, G. A. Petersson, H. Nakatsuji, M. Hada, M. Ehara, K. Toyota, R. Fukuda, J. Hasegawa, M. Ishida, T. Nakajima, Y. Honda, O. Kitao, H. Nakai, M. Klene, X. Li, J. E. Knox, H. P. Hratchian, J. B. Cross, C. Adamo, J. Jaramillo, R. Gomperts, R. E. Stratmann, O. Yazyev, A. J. Austin, R. Cammi, C. Pomelli, J. W. Ochterski, P. Y. Ayala, K. Morokuma, G. A. Voth, P. Salvador, J. J. Dannenberg, V. G. Zakrzewski, S. Dapprich, A. D. Daniels, M. C. Strain, O. Farkas, D. K. Malick, A. D. Rabuck, K. Raghavachari, J. B. Foresman, J. V. Ortiz, Q. Cui, A. G. Baboul, S. Clifford, J. Cioslowski, B. B. Stefanov, G. Liu, A. Liashenko, P. Piskorz, I. Komaromi, R. L. Martin, D. J. Fox, T. Keith, M. A. Al-Laham, C. Y. Peng, A. Nanayakkara, M. Challacombe, P. M. W. Gill, B. Johnson, W. Chen, M. W. Wong, C. Gonzalez, and J. A. Pople, *Gaussian, Inc., Pittsburgh PA, 2003*